NUKLEONIKA 2021;66(4):159–164
doi: 10.2478/nuka-2021-0024

ORIGINAL PAPER

sciendo

Sub-cellular elemental imaging of human muscle tissues affected by neuromuscular diseases

Patrycja Śliż-Szpytna, Marek Lankosz, Joanna Dudała, Dariusz Adamek, Edyta Radwanska, Borys Kwinta, Milko Jakšić, Iva Božičević Mihalić, Georgios Provatas

Abstract. Various types of neuromuscular diseases differ in symptoms, pathology, and clinical picture but one of their common elements is muscle weakness, which could lead to human motor activities impairment and in many cases to shortening of life span and even death due to respiratory failure. That is why it is very important to better understand the underlying causes of these diseases to be able to implement new methods of treatment more effectively. This paper presents the results of the elemental analysis of human muscular tissues affected by dystrophy and myopathy. For this purpose, the particle-induced X-ray emission method was used, which is perfectly suited for measuring light elements. The samples were analysed for differences in the elemental composition of Na, Mg, P, S, Cl, K, Fe, Zn, and Br. The results were presented in the form of elemental concentration maps and a thorough statistical analysis of the obtained data using the advanced statistical methods.

Keywords: Dystrophy • Elemental analysis • Myopathy • Neurodegenerative diseases • PIXE

P. Śliż-Szpytna✉, M. Lankosz, J. Dudała
AGH University of Science and Technology
Faculty of Physics and Applied Computer Science
Mickiewicza 30 Ave., 30-059 Krakow, Poland
E-mail: slizpatrycja@gmail.com

D. Adamek, E. Radwanska
Jagiellonian University
Faculty of Medicine
Chair of Pathomorphology
Grzegórzecka 16 Str., 31-531 Krakow, Poland

B. Kwinta
Jagiellonian University Medical College
Department of Neurosurgery and Neurotraumatology
Botaniczna 3 Str., 31-503 Krakow, Poland

M. Jakšić, I. Božičević Mihalić, G. Provatas
Ruđer Bošković Institute
Bijenička cesta 54, 10000, Zagreb, Croatia

Received: 29 December 2020
Accepted: 12 March 2021

Introduction

Neuromuscular diseases essentially incorporate motor neuron disorders, diseases of nerve–muscle junction, neuropathies, and myopathies whose primary and characteristic feature is direct damage to muscle tissue. In many cases, to diagnose myopathy and determine its cause, a muscle biopsy is performed, especially when clinical symptoms, biochemical, and genetic tests are not conclusive. In the pathomorphological diagnosis, morphological features, metabolic and immunohistochemical profile are taken into account. The lack of effective therapy of many of neuromuscular diseases is due to insufficient knowledge of the pathomechanism of the disease. Currently, a lot of scientific research is carried out to better understand this disease and implement new methods of treatment. The limited number of effective therapies has resulted in a large number of studies carried out in this area [1, 2].

Current hypotheses indicate the participation of processes like oxidative stress, excitotoxicity, peroxide dismutase, etc., which lead to biochemical and, subsequently, functional and morphological changes [3, 4]. It seems that the elemental changes in muscle fibers can reflect important processes or even be helpful in diagnosis.

Particle-induced X-ray emission (PIXE) provides the ability of getting inside the potential changes in chemical composition (elemental composition and molecular structure analysis) of muscle tissue that manifests features of neuromuscular disease.

The paper aims to provide a better understanding of myopathy, which, in the future, may result in effective prevention of disease or slowing down the progress of disease, or if not, even finding a new effective method of treatment.

Methodology

The samples were prepared and diagnosed at the Department of Neuropathology of Collegium Medicum Jagiellonian University, Krakow, Poland. Tissue materials were shock-frozen with liquid C_3H_8. For each specimen, two adjacent tissue slices were cut into 8 μm on the cryomicrotome. One slice was placed on the microscope and used for histological purposes. Consecutive slice was mounted on a silicon nitride window (nitride thickness: 200 nm, window size: 2 × 2 mm^2) for PIXE analysis. The samples for elemental measurements were freeze-dried. Before deciding to include a given case for investigation, in each case, the appropriate examination using standard methods was applied in myopathology; histochemical and immunohistochemical staining were also performed.

Measured samples were split into three categories: control (muscle biopsy without pathological evidences of the diseases), dystrophy (limb girdle muscular dystrophy) and myopathy (unspecified, either primary or secondary even neurogenic). The measurements were conducted at the Ruder Boskovic Institute in the Laboratory for Ion Beam Interaction, Zagreb, Croatia. In the measurements a 1 MV Tanderon accelerator was used. The samples were measured at the cellular level with the use of a fine focused ion microbeam with a proton energy up to 2 MeV. For elemental analysis PIXE technique was applied. PIXE spectra were collected using Princeton Gamma-Tech Institute (PGT) 30 mm^2 area Si(Li) detector with a 12.5 μm Be window placed at 135° relative to the beam direction at a distance of about 4 cm from the target. The sample was mounted on a cold finger and cooled using a liquid nitrogen cryostat. The silicon frame was mounted on a sample holder with the use of scotch tape covered with carbon. As a result, charging of the irradiated samples with an electric charge was avoided. The PIXE measurements were combined with the registration of the energy of particles after passing through the sample, which is performed using scanning transmission ion microscopy (STIM) and provides information on the surface density. The sample was excited with beam dimensions of ca. 1 × 1 μm^2. Off-axis STIM maps were measured with use of a 300 μm thick passivated implanted planar silicon (PIPS) detector placed at around 25° off the beam axis. The details of measuring chamber have been presented in Fig. 1.

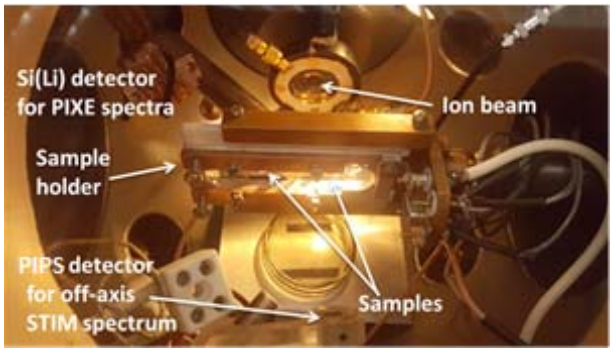

Fig. 1. View of the measuring chamber.

Results and discussion

During the analysis, the samples were divided into three categories: control, myopathy, and dystrophy with appropriate abbreviations that will appear later in the article consecutively labelled (C, M, and D). During the interpretation of the obtained results, the emphasis was put mainly on the measurements made in the areas of single muscle fibers; measurement points can be a valuable source of information about the fiber without "contamination" by surrounding endomysial connective tissue or other cellular components. Using the PyMca [5] software, the numerical values of the intensity distribution of individual elements such as Na, Mg, P, S, Cl, K, Fe, Zn, and Br were obtained. To present maps of the elemental distribution, appropriate scripts were written in Python.

In the first step, a preliminary scan of the muscle tissues was performed using the STIM method; as a result, visual information about the elemental appearance of the surface was obtained. Then a scan with a constant resolution of 128 pixels × 128 pixels was performed using the PIXE method (the dimensions of one pixel for every single measurement were 2.73 × 2.73 μm^2). The average duration of the measurement was approximately 8.2 s/px, while the used beam current was ca. 500 pA. In the next step, three interesting places in the muscle tissues were chosen, where especially precise point measurements were made. In this type of measurement, the scanning resolution was the same as described previously.

Initially, a STIM scan was performed to select the appropriate measurement place on one of the control samples. An optical microscope photo with the STIM image imposed on is shown in Fig. 2. This allowed for the distinction of individual muscle fibers. It was a critically important step because, after the PIXE scan with a size of 350 × 350 μm^2, point scans were performed within individual muscle fibers. Several maps for selected elements of the control sample are presented in Fig. 3. The scanning system used during measurements has an expeditious scanning beam that proceeds in horizontal and vertical directions while the sample is fixed. In that way, sample during one measurement is scanned numerous times to obtain satisfactory statistics. The size of the measured point 1 was 12 pixels × 11 pixels, point 2 was 14 pixels × 12 pixels, and point 3 was 15 pixels × 13 pixels. Distinct muscle fibers

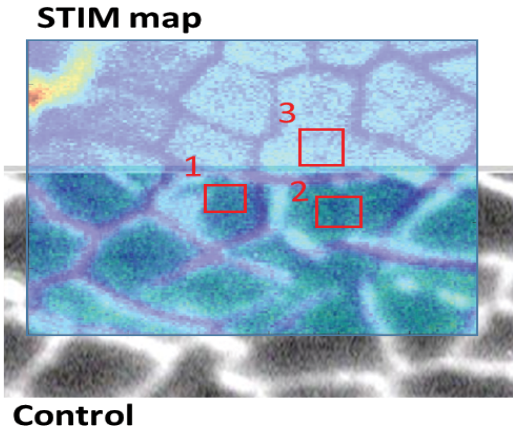

Fig. 2. Optical microscope photo with superimposed STIM image. The red rectangles on the image represent the scan areas of point measurements for control sample.

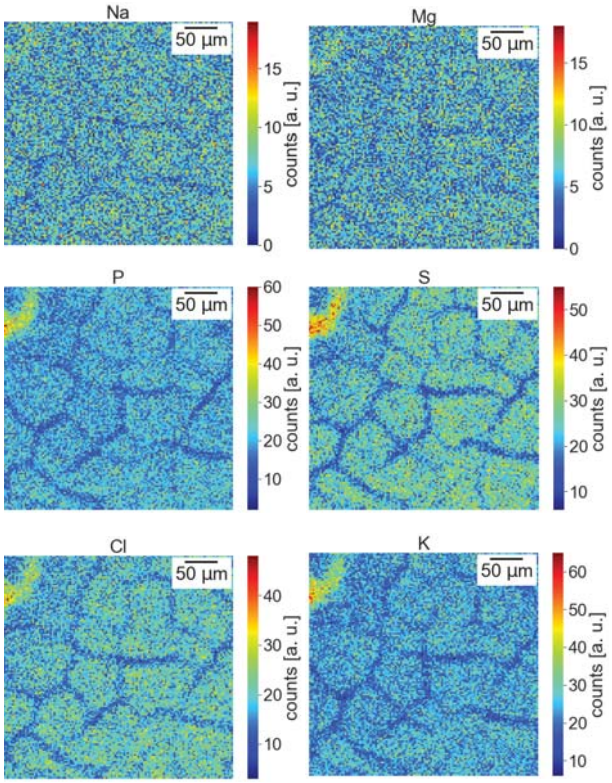

Fig. 3. Element distribution maps of control sample made with the PIXE method.

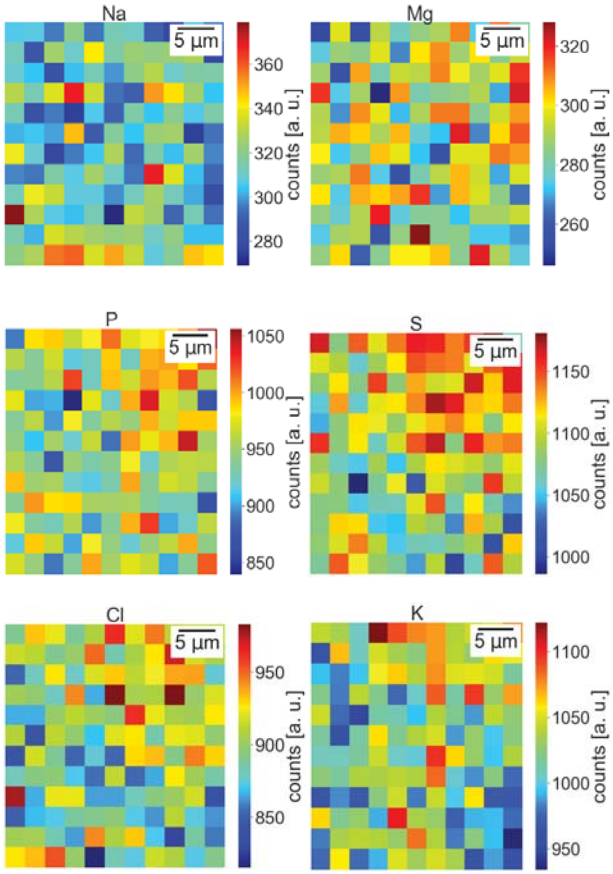

Fig. 4. Maps of the elemental distribution of point no. 1 located on control sample.

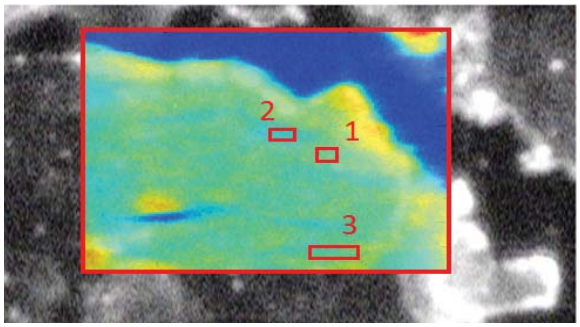

Fig. 5. Optical microscope photo with superimposed STIM image. The red rectangles on the image represent the scan areas of point measurements for dystrophy sample.

borders are noticeable, especially for P, S, Cl, and K. Figure 4 shows exemplary maps of elementary distribution for point 1 selected on the basis of a tissue scan using the STIM method.

The measurements of the dystrophic sample were made in the same way as for the control sample. The image representing the measured areas for this sample is presented in Fig. 5. It should be mentioned that, in this case, the distinction between individual muscle fibers was not as obvious as in the case of the control sample, as shown in Fig. 6. The sizes of individual points were, respectively, point no. 1 – 6 × 6 pixels, no. 2 – 6 × 9 pixels, and no. 3 – 8 × 17 pixels. The point measurement for this sample in point 3 was highly interesting, because for two elements (iron and zinc) an increased concentration was noticed in the same place. This is likely due to local aggregation of myoglobin, resulting from subcellular damage to the muscle, which is coupled to another zinc compound-forming protein [6].

For the myopathy sample, measurements were made in the same way as for the control sample and for the dystrophic sample. In this case, the size of the spot measurement areas had 10 × 18 pixels and 13 × 37 pixels.

The presented maps show significant diversifications in elemental distributions depending on the structure of the tissue. It was discovered that Na, Mg, P, S, Cl, and K are distributed in all fibers and are having higher concentrations. However, spots containing Fe, Zn, and Br were also found, as presented in Fig. 7.

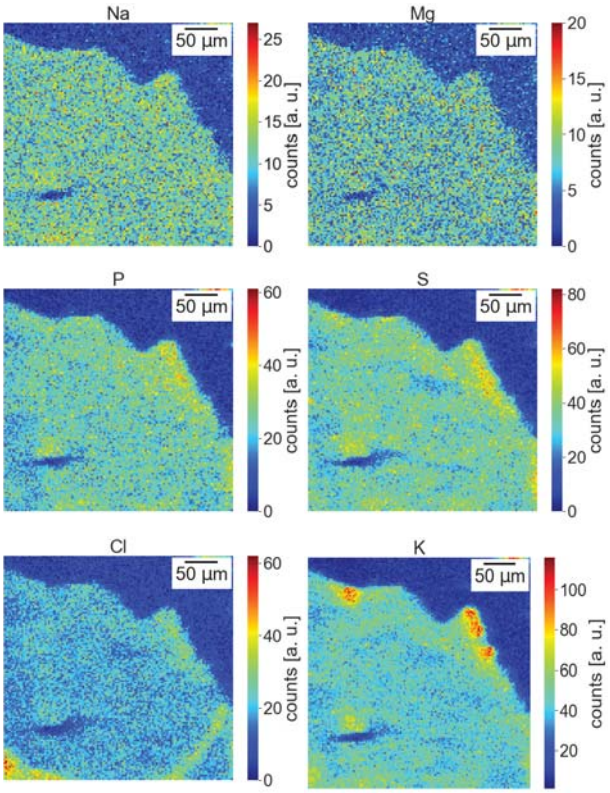

Fig. 6. Element distribution maps of dystrophy sample made with the PIXE method.

All statistical calculations were performed with the Statistica 13 software [7]. In the analyses, mainly point data were used, as they were considered to provide the best source of information about both healthy and diseased muscle tissues.

Since the base on which the sample was located during the measurements in the measuring chamber was made of silicon nitride and the beam current during the measurements was not stable, normalization was done by the value of counts for Si for each measurement.

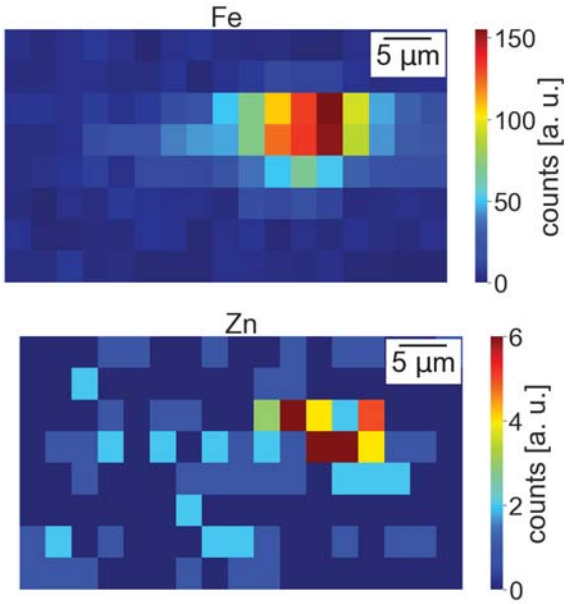

Fig. 7. Selected maps of the elemental distribution for point no. 3 – dystrophy sample.

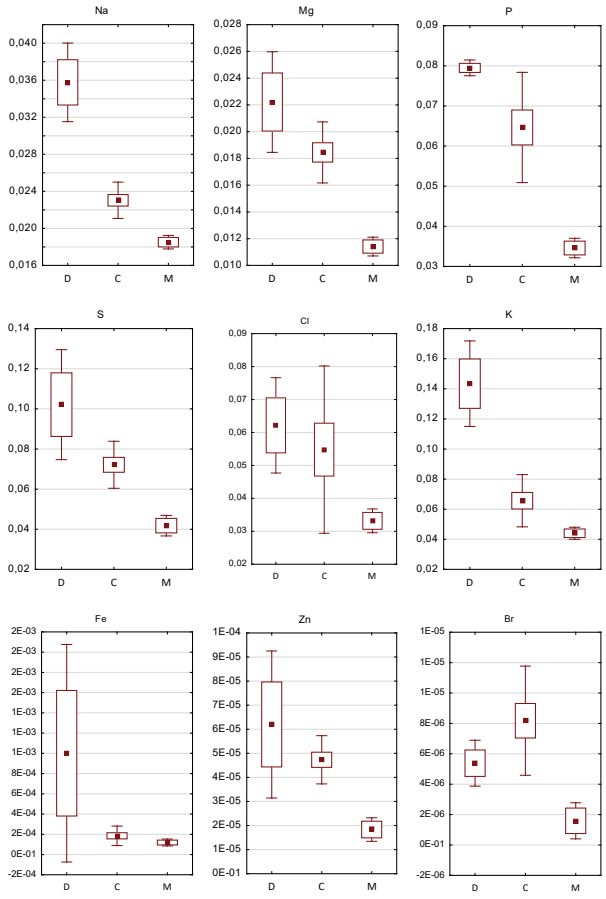

Fig. 8. Box-and-whisker plots for the Kruskal–Wallis test for individual elements with mean values (inner box), means ± standard error (outer box), and means ± standard deviation (whiskers).

As the statistical normality test was not met for the obtained data, the parametric statistics could not be used. Therefore, the non-parametric Kruskal–Wallis test was performed and presented in the form of graphs in Fig. 8. There are noticeably significant differences between disease states and control, especially for such elements as Na, Mg, P, S, Zn, and Br.

The U Mann–Whitney test was also performed for pairs of groups M-C, M-D, and C-D. He showed the significance of Na, Mg, P, and S for the M-C pair, and Na, K, and Fe for the D-C pair. Significance was determined based on the value of the p parameter, which was 0.05. Values below this number were considered statistically significant.

The multivariate discriminant analysis (MDA) progressive step procedure was used, which allowed for entering successive variables with the highest discriminant power to the model. The Wilks' lambda was determined for the variables, and the obtained values are given in Table 1. The lower

Table 1. Partial Wilks' lambda values

Partial Wilks' lambda								
K	S	Na	Cl	P	Mg	Zn	Fe	Br
0.24	0.70	0.95	0.59	0.65	0.93	0.99	0.99	0.99

the parameter value, the greater is the significance of the element in tissue classification. Based on this, it can be concluded that the elements with the highest significance are K, Cl, P, and S.

From this analysis, discrimination functions were obtained, which are linear combinations of characteristic X-ray intensities of the elements considered in the model. From all the obtained functions, we selected those that offered the best differentiation between samples. Concentrations of elements are represented in the formulae by their symbols:

$$(1) \quad D_1 = 2.269\,K - 1.200\,S + 0.286\,Na - 2.148\,Cl + 1.654\,P - 0.333\,Mg - 0.067\,Zn - 0.036\,Fe - 0.041\,Br$$

$$(2) \quad D_2 = -0.577\,K + 0.963\,S - 0.90\,Na - 1.413\,Cl + 1.440\,P + 0.367\,Mg + 0.071\,Zn - 0.066\,Fe + 0.040\,Br$$

The first function is mostly affected by the coefficients of the following elements: K, Cl, P, and S. In the second function, the main components are also the coefficients of the four elements mentioned concerning the D_1 function; only in this case, the influence of individual elements differs from the previous one. This time, chlorine has the greatest influence. The comparison of these two functions with each other in a graphical form is presented in Fig. 9.

The graph clearly shows that the coordinates of the vast majority of points representing sample D concerning the first discriminant variable D_1 have much higher values than the analogous coordinates of points representing, respectively, samples C and M. Additionally, the coordinates of points representing sample M for the first discriminant variable take values from the lower half part of the coordinate variation interval for sample C. Due to the smaller discrimination of the samples to the second discriminant variable, their ranges of coordinate variability begin to overlap significantly. Due to the data overlap, another MDA analysis was performed, this time separating the two control samples to determine what the cause of this data overlap could be.

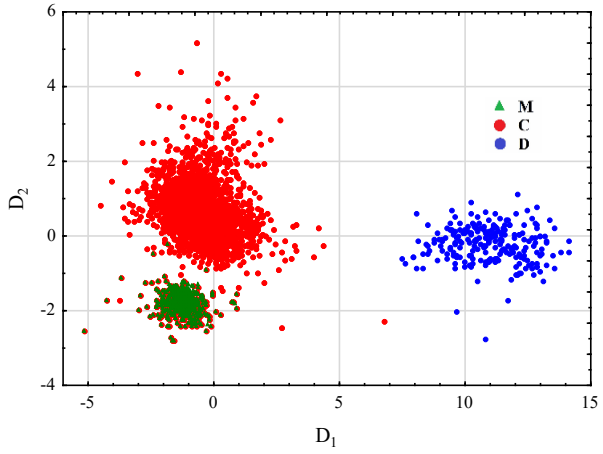

Fig. 9. A graph of the configuration of points representing three types of muscle tissue samples in a layout determined by discriminant variables (axes).

Interestingly, one of the control samples was rather in agreement with myopathy that to second control case. Her microscopic diagnosis was ambiguous; so, it was originally decided to assign her to the control group. In fact, neuropathological revision of this biopsy material revealed extremely scarcely noticeable traces of pathological changes.

Conclusions

Neuromuscular diseases, especially myopathies, are very difficult to be diagnosed quickly and unambiguously. The knowledge of the pathogenesis is far from being satisfactory; however, the elemental changes within the muscle fibers might bring some valuables from the point of diagnostic and clinical issues. For this reason, these studies have been devoted to try to observe elemental differences, in particular broad categories of muscle pathology, especially regarding dystrophy and myopathy. Elemental distribution maps were created using the PIXE method, which allowed for the observation of elemental differences in each of the described states. The following statistical analyses were carried out: Kruskal–Wallis test, U Mann–Whitney test, and MDA; further, Wilks' lambda was designated. The first two statistical methods emphasized the importance of elements such as Na, Mg, P, and S in creating distinctive pattern or pathology.

The MDA analysis made it possible to distinguish samples in terms of the concentration of elements, emphasizing the importance of such elements as K, Cl, P, and S. Moreover, due to the overlapping of graphical data obtained by canonical analysis represented by the control samples and the myopathy sample, it was decided to further conduct deeper analysis of the cause of this situation. After another more detailed analysis of the MDA, it turned out that one sample was consistent in value with the myopathy sample. One of the reasons for this may be the fact that the sample diagnosed as the control may have already had initial symptoms of neuromuscular disease that were not clearly discernible neuropathologically. This is only a preliminary thesis, which will require further research in this field.

Acknowledgments. The authors acknowledge the support provided by the IAEA within the framework of a Coordinated Research Project G42008 on "Facilitating Experiments with Ion Beam Accelerators".

ORCID

D. Adamek http://orcid.org/0000-0002-5570-2259
I. Božičević Mihalić http://orcid.org/0000-0002-0221-4024
J. Dudała http://orcid.org/0000-0002-5699-3959
M. Jakšić http://orcid.org/0000-0002-6750-9990
B. Kwinta http://orcid.org/0000-0002-3807-5775
M. Lankosz http://orcid.org/0000-0003-3126-9806
P. Śliż-Szpytna http://orcid.org/0000-0001-5271-891X

References

1. Tabebordbar, M. S., Wang, E. T., & Wagers, A. J. (2013). Skeletal muscle degenerative diseases and strategies for therapeutic muscle repair. *Annu. Rev. Pathol.-Mech. Dis.*, *8*, 441–475. DOI: 10.1146/annurev-pathol-011811-132450.
2. Katirji, B., Kaminski, H. J., & Ruff, R. L. (2014). *Neuromuscular disorders in clinical practice*. New York: Springer-Verlag.
3. Becker, R. A., Cluff, K., Duraisamy, N., Casale, G., & Pipinos, I. (2017). Analysis of ischemic muscle in patients with peripheral artery disease using X-ray spectroscopy. *J. Surg. Res.*, *220*, 79–87. DOI: 10.1016/j.jss.2017.06.073.
4. Gautam, R., Vanga, S., Madan, A., Gayathri, N., Nongthomba, U., & Umapathy, S. (2015). Raman spectroscopic studies on screening of myopathies. *Anal. Chem.*, *87*, 2187–2194. DOI: 10.1021/ac503647x.
5. Sole, V. A., Papillon, E., Cotte, M., Walter, Ph., & Susini, J. (2007). A multiplatform code for the analysis of energy-dispersive X-ray fluorescence spectra. *Spectroc. Acta Pt. B-Atom. Spectr.*, *62*, 63–68. DOI: 10.1016/j.sab.2006.12.002.
6. Lynch, S. A., McLeod, M. A., Orsech, H. C., Cirelli, A. M., & Waddell, D. S. (2019). Zinc finger protein 593 is upregulated during skeletal muscle atrophy and modulates muscle cell differentiation. *Exp. Cell Res.*, *383*, 111563. DOI: 10.1016/j.yexcr.2019.111563.
7. TIBCO Software Inc. (2017). Statistica (data analysis software system), version 13. http://statistica.io.